6

DYNAMIC QUENCHING IN SINGLE PHOTOSYSTEM II SUPERCOMPLEXES

Photosystem II (PSII) is a huge pigment–protein supercomplex responsible for the primary steps of photosynthesis in green plants. Its light-harvesting antenna exhibits efficient transfer of the absorbed excitation energy to the reaction center and also contains a well-regulated protection mechanism against over-excitation in strong light conditions. The latter is based on conformational changes in antenna complexes that open up excitation decay channels resulting in considerable fluorescence quenching. Meanwhile, fluorescence blinking, observed in single antennas, is likely caused by a similar mechanism. Thus the question arises whether this effect is also present in and relevant to the native supramolecular organization of a fully assembled PSII. To further investigate energy transfer and quenching in single PSII, we performed single-molecule experiments on PSII supercomplexes at 5°C. Analysis of the fluorescence intensity and mean lifetime allowed us to distinguish detached antennas and specifically analyze PSII supercomplexes. The average fluorescence lifetime in PSII of about 100–150 ps, measured under our extreme excitation conditions, is surprisingly similar to published ensemble lifetime data of photochemical quenching in PSII of a similar size. In our case, this lifetime is nevertheless caused by either one or multiple quenched antennas or by a quencher in the reaction center. The observed reversible light-induced changes in fluorescence intensity on a millisecond timescale are reminiscent of blinking subunits. Our results therefore directly illustrate how environmental control over a fluctuating antenna can regulate light-harvesting in plant photosynthesis.
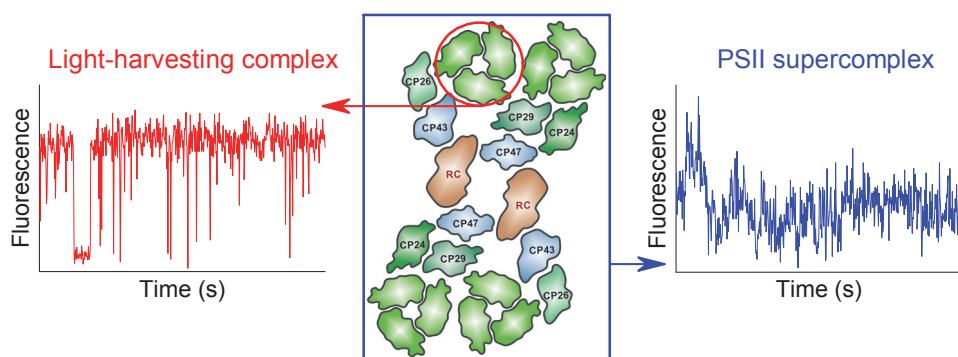
Figure 6.1: Table of contents graphic

6.1 INTRODUCTION

The main function of photosystem II (PSII) is to absorb light by its light- harvesting antenna and then to transfer the generated electronic excitation to the reaction center (RC), where it is used to oxidize water and separate a free electron, thus initiating the chain of photochemical processes. One of the most puzzling questions in this primary light reaction of photosynthesis concerns the regulation of light-harvesting in PSII in plants by non-photochemical quenching (NPQ)—the process of dissipation of excess excitation energy under strong sunlight via mechanisms different from photochemical quenching taking place in the RC [197]. A major part of NPQ is the so-called energy-dependent quenching (qE) that is sensitive to pH variations and can be reversibly activated on a timescale of several seconds to minutes [166]. There is wide consent that qE takes place in the peripheral antenna of PSII, but the precise location and molecular mechanism remain under debate (for reviews, see [26–28]). The rate of charge separation in the RC, on the other hand, depends on the redox state of the primary quinone acceptor Q [198]. In closed RCs, the rate of charge separation is slowed down significantly due to the electrostatic effect of Q_A^-, so electronic excitations remain in the antenna of PSII with an unquenched excited state lifetime of more than 2 ns [132]. Therefore, closing of RCs results in a significant increase in the fluorescence intensity that is utilized in a variety of methods to study the properties of functional PSII preparations, chloroplasts, or even whole plants [199].

One of the complications in the investigation of qE via fluorescence spectroscopy is the convolved effect of the variable fluorescence and excited state

quenching with the structural and spatial component of energy transfer in PSII. The fluorescence decay of PSII can be described by a sum of exponential decays [20, 22], but that does not allow finding a unique mechanistic description of the self-regulation ability of PSII [110]. Recent models of excitation energy transfer in PSII also account for fluctuating properties of the light-harvesting antenna system, arising either from the dynamically varying inter-complex energy transfer rates [94, 200] or from conformational switching of individual antennas between their several functionally distinct states [201], as has been observed by single-molecule spectroscopy (SMS) [78, 118, 202].

Structurally, PSII consists of a homodimeric core complex that contains the photochemically active RC and the catalytic oxygen-evolving complex [4]. The core further accommodates the inner antennas CP43 and CP47. The dimeric core of PSII in the thylakoid membrane is surrounded by the peripheral antenna system comprised of the minor light-harvesting antenna complexes (LHC) CP24, CP26 and CP29 and multiple trimeric light-harvesting complexes II (LHCIIs) [6, 8], see Fig. 6.8 in the Supporting Information (SI) for a schematic illustration. PSII supercomplexes with this supramolecular organization can be biochemically isolated in various sizes [10]. A $C_2S_2M_2$ supercomplex is, for example, comprised of the dimeric core (C_2), two strongly bound LHCII trimers (S_2), two moderately bound LHCII trimers (M_2) plus the minor LHCs. PSII contains hundreds of chlorophyll (Chl) pigments that efficiently transfer the absorbed energy to the RC [16, 18]. Additional carotenoid pigments not only increase the overall spectral absorption range, but also provide a vital photoprotective mechanism via quenching of Chl triplet states that are generated under conditions of closed RCs. Indeed, in the absence of photochemistry, the high rate of intersystem crossing in Chls in a protein environment results in a triplet state yield of about 30% [12]. Chl triplets interact readily with molecular oxygen to form highly reactive and toxic oxygen species. Therefore, to avoid possible photodamage, these Chl triplets are efficiently quenched by Cars to form Car triplet states that then safely dissipate their energy as heat in a few microseconds [58]. Moreover, Cars are also supposed to participate in the qE part of NPQ [26].

Single-molecule spectroscopy (SMS) on isolated LHCs has shown the presence of significant fluorescence intensity and lifetime dynamics under conditions mimicking NPQ *in vivo* [78, 118]. These results suggest that the observed fluorescence intermittency in those isolated LHCs originates from intrinsic conformational changes that correspond to the same molecular mechanisms regulated by qE in the native system [37]. Recent ultra-fast ensemble spectroscopy [117] and modeling fit with that interpretation [61, 62, 120]. In the quest to

test that hypothesis for the light-harvesting complexes embedded in a supra-molecular PSII arrangement, we performed SMS on isolated PSII supercomplexes [10]. The strong non-physiological illumination necessary to observe single PSII supercomplexes poses a challenge to correctly interpret the fluorescence data. Here we report and identify the quenched fluorescence characteristics of single PSII supercomplexes. We utilize modulated laser excitation to probe for quenching species in the micro- and millisecond time range and analyze the observed data using a coarse-grained modeling for energy transfer and fluorescence quenching in a fluctuating antenna. We identify the underlying quenching mechanisms and discuss their implications.

6.2   MATERIALS AND METHODS

Sample preparation

Monomeric CP24 and trimeric LHCII complexes were isolated from the thylakoid membranes of *Arabidopsis thaliana* as described earlier [194]. The purification of $C_2S_2M_2$ supercomplexes of PSII in *Arabidopsis thaliana* was performed according to the protocol described by Caffarri et al. [10]. C_2S_2 supercomplexes were isolated from the CP24ko mutant because the outer M-trimers do not bind to PSII in the absence of CP24 [203]. This procedure resulted in a more homogeneous size distribution. The sample was diluted in 30 mM Hepes and 0.008% (w/v) dodecyl-α-D-maltoside (α-DM) at pH 7.5 to a picomolar concentration range and then immobilized on a poly-L-Lysine coated cover glass [47]. The density of surface bound complexes was adjusted to about 10 complexes per $100\,\mu m^2$.

Single-molecule spectroscopy and data analysis

The fluorescence emission of single particles was measured with a confocal epifluorescence microscope. The sample was cooled to 5°C and solubilized oxygen was scavenged using the enzyme mix 25 nM protocatechuate-3,4-dioxygenase and 2.5 mM protocatechuic acid (Sigma Aldrich) to improve the photo-stability of complexes. A Ti:sapphire laser (Coherent MIRA 900F) with a pulse width of about 200 fs and a repetition rate of 76 MHz, coupled to a tunable optical parametric oscillator (Coherent MIRA OPO), provided excitation light at a wavelength of 633 nm. The polarization was set to near-circular using a Berek polarization compensator (New Focus). A motorized flipping mirror in the detection path was used to either perform wavelength integrated single photon

counting with an avalanche photodiode (PDM 20 μm, MPD) or to measure the fluorescence spectrum. The spectrum with one second integration time was obtained by dispersing the fluorescence via a grating (HR830/800nm, Opto-metrics LLC) onto a CCD camera (Spec10:100BR, Roper Scientific). The absolute and relative arrival time of photons detected with the MPD and fluorescence decay histograms were measured with a time correlated single photon counting (TCSPC) device (PicoHarp 300, PicoQuant). Fluorescence intensity traces with a binning time of 10 ms were analyzed with a custom MATLAB code to identify stable intensity levels, as described earlier [83]. The fluorescence decay of one intensity level was binned into 4 ps time intervals, background corrected by subtracting a measured and time weighted background signal and then further analyzed with the fitting software FluoFit (PicoQuant). A two-exponential reconvolution fit yielded the decay times, amplitudes and the corresponding amplitude-averaged lifetime. The instrument response function (IRF) with a FWHM of 38 ps was measured from scattered light at the peak emission wavelength of PSII ($\lambda = 681\,$nm). The lack of structure in the fit residuals and their auto-correlation function indicated a satisfying fit.

Pulse wave excitation

An acousto-optic modulator (AOM, MT350, Acousto-Optic Devices) was placed in the pulsed laser beam path to effectively act as a fast shutter in the microsecond and millisecond range to probe and observe the accumulation and decay of quenchers on the corresponding timescales. The generated excitation pulse waves are described by the period and pulse duration of one modulation cycle. The absolute arrival time of detected fluorescence photons can be projected back in one modulation cycle which allows us to build up a photon arrival time histogram (AOM delay time histogram) that describes the fluorescence intensity kinetics within one modulation cycle. The inset in Fig. 6.4 illustrates such an envelope modulation with a period T and a pulse duration τ. The exemplary arrival time of a fluorescence photon with respect to the excitation modulation is indicated as the AOM delay time t. The off-time of the excitation light is then given as $t_{\text{off}} = T - \tau$.

Monte-Carlo simulations of excitation dynamics

The simple kinetic approach usually used to model excitation dynamics in various systems cannot adequately describe the non-linear processes of excitation relaxation, like S–T or S–S annihilation, occurring in small molecular aggreg-

ates. Instead, more sophisticated statistical models were developed [75, 76, 91, 106]. Their application to a single PSII supercomplex, where excitation migration through the antenna should be implicitly taken into account, however, is very limited. Therefore, in order to deal with both effects (excitation migration and non-linear annihilation), we used a Monte-Carlo approach to simulate fluorescence blinking in a single PSII supercomplex arising due to a random generation of the triplet states and the static traps resembling NPQ quenchers observed *in vivo*. A detailed description of the modeling procedure is presented in the SI.

6.3 EXPERIMENTAL RESULTS

SMS measurements and fluorescence kinetics in the ns time range

The observed fluorescence intensities (*cf.* Fig. 6.2) and fluorescence spectra (*cf.* Fig. 6.9 in the SI) of single PSII supercomplexes are comparable to those of isolated light-harvesting antennas. These similarities complicate the analysis of the sample, especially because the M trimers and the minor CP24 monomers often detach from the larger C_2S_2M and $C_2S_2M_2$ particles. Additional information about the fluorescence lifetime, however, allows us to distinguish isolated antennas from PSII complexes: the former exhibit mainly a slow fluorescence decay in the ns range while the latter show a much faster average fluorescence lifetime of about 100–150 ps, as demonstrated in the inset of Fig. 6.2B for an acquisition time of 60 s. This difference in mean fluorescence lifetimes counteracts the difference in absorption cross-sections and results in the mentioned similarity of the detected fluorescence intensity. The exact difference in fluorescence intensity strongly depends on the used excitation intensity due to exciton annihilation effects [68]. The time traces of the fluorescence intensity and average lifetimes, shown in Fig. 6.2, were measured at an excitation intensity of $75\,W/cm^2$, which corresponds to 10^4 absorbed photons per second per chlorophyll. For a detached antenna, this excitation power resulted in an average lifetime of ~1.7 ns, which together with the absolute fluorescence intensity matches the expected values for an LHCII trimer [106]. In addition to the unquenched lifetime of about 3.5 ns, the singlet–triplet (S–T) annihilation process causes the appearance of a second lifetime component of 35 ps with an amplitude ratio of about 50/50 (*cf.* inset in Fig. 6.2A). The fluorescence decay kinetics of PSII supercomplexes was also fitted with two exponential components—a dominating one in the range of 100 ps and a less pronounced component accounting for

slower kinetics up to 3.5 ns. The distributions of these two lifetimes and their relative amplitudes are shown in Fig. 6.10 in the SI.
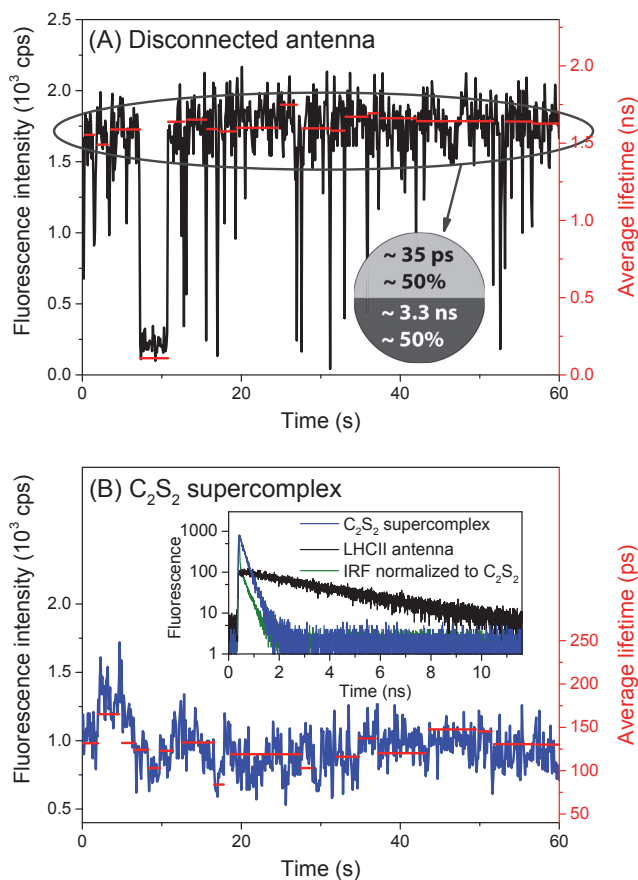

Figure 6.2: Fluorescence intensity traces of a detached antenna (black line in A) and a C_2S_2 supercomplex (blue line in B). The fitted average lifetime of individual intensity levels is plotted in red for both graphs. The average fluorescence lifetime of an un-quenched level of antenna complexes is comprised of the intrinsic singlet excited state decay in the ns range and an annihilation artifact of 35 ps (gray circle in A). The corresponding fluorescence decay histograms of A and B, accumulated over 60 s, are shown in the inset of B on a semi-logarithmic scale using the same color scheme. The instrument response function with a FWHM of 38 ps is depicted in green and normalized to the decay of C_2S_2 for better comparison.

Determining the absorption cross-section

Measurements of the absolute fluorescence intensity of a complex together with its average lifetime allows us to estimate the relative absorption cross-section [108, 202] and therefore to quantitatively distinguish larger PSII units from isolated antennas, detached during sample preparation. A distribution of these distinct sample clusters is shown in Fig. 6.11 in the SI. For reference, we have also measured the distribution of the absorption cross-section of LHC monomers, trimers, and pentamers (LHCII trimer with CP24 and CP29 minors attached) [204], that all can be clearly distinguished from C_2S_2 supercomplexes, see Fig. 6.12 in the SI. Indeed, at an excitation wavelength of 633 nm Chls *a* and *b* absorb about the same amount of photons. Thus the absorption cross-section of C_2S_2 supercomplexes corresponds to about 210 Chls (10 LHC monomers contain about 14 Chls and two core complexes about 35 Chls), while an LHCII trimer contains just 42 Chls. The ratio of these Chl numbers corresponds reasonably well to the relative absorption cross-sections shown in Fig. 6.12 in the SI.

In order to check the dependence of the fluorescence lifetime of PSII super-complexes on the particle size, we also measured larger $C_2S_2M_2$ particles. The results are summarized in Fig. 6.3. As expected, the distribution of absorption cross-section of $C_2S_2M_2$ supercomplexes (green bars) is indeed shifted to larger values compared to C_2S_2 particles (blue bars). Moreover, the broader distribution in the case of $C_2S_2M_2$ supercomplexes indicates a more inhomogeneous sample composition, and there is indeed a significant fraction of detached antennas present (black bars), which exhibit the absorption cross-section of mostly trimeric complexes with an average lifetime of about 1.5 ns. There are also some monomeric antennas present with even longer average lifetime due to less pronounced S–T annihilation. Meanwhile, the mean lifetime in PSII super-complexes has been shown to increase with larger PSII assemblies due to the significant contribution of excitation migration through the antenna [20]. Our results for $C_2S_2M_2$ complexes are only marginally shifted to longer decay times (possibly due to the sample inhomogeneity).

The average fluorescence lifetime in PSII supercomplexes is surprisingly similar to that observed in ensemble measurements on PSII complexes with open RCs (when excitation intensity is about 0.1 mW/cm^2), even though the necessary excitation intensities in SMS are 4 orders of magnitude higher [20, 22]. This mean lifetime further depends on the excitation intensity, as depicted in Fig. 6.13 in the SI, and significantly decreases at excitation intensities above 75 W/cm^2 due to the increased probability of S–T and singlet–singlet (S–S)
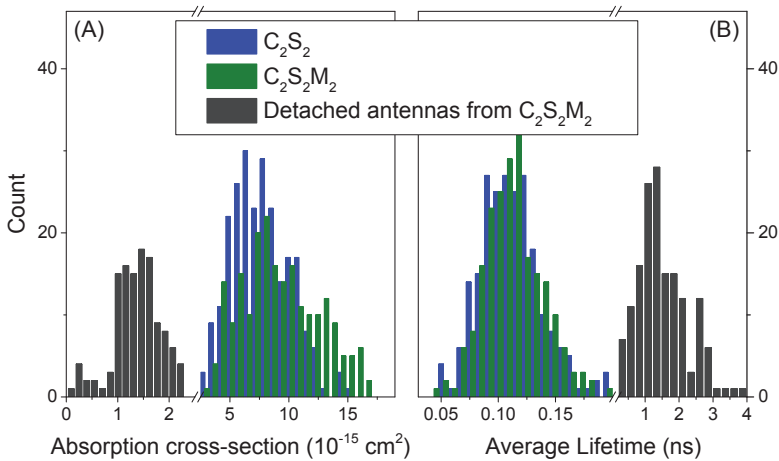
Figure 6.3: Histogram distributions of the calculated relative absorption cross-section (A) and the corresponding average lifetime (B) of C_2S_2 (blue bars) and $C_2S_2M_2$ (green bars) supercomplexes as well as the detached antennas found in the $C_2S_2M_2$ sample (black bars). Note the break and change in scaling on the x-axis of both panels. The histograms were obtained by analyzing individual intensity states, *i.e.* stable intensity levels with sufficient photon counts (>2000 counts), of multiple individual particles: 30 C_2S_2 complexes, 42 $C_2S_2M_2$ complexes and 22 detached antennas.

annihilation. By using the experimentally determined absorption cross-section of about $\sigma = 7 \cdot 10^{-15}$ cm^2 for a C_2S_2 supercomplex and an excitation intensity of 500 W/cm^2, the chance for the generation of two excitations per PSII per pulse does not exceed 2%. Below that excitation intensity S–S annihilation can therefore be neglected. To check the quantum yield of the S–T annihilation and to investigate the nature of the fluorescence quenching, we also performed time-resolved excitation modulation experiments to probe the accumulation and decay kinetics of the quencher(s).

Modulated fluorescence kinetics in the micro- and millisecond time range

Microsecond time scale.

In previous work we showed the influence of S–T annihilation on the fluorescence decay of photosynthetic LHCs [106]. Here, we utilized the same laser modulation technique *via* an acousto-optic modulator (AOM) to check for the presence and accumulation of Car triplets in PSII supercomplexes (see the inset in Fig. 6.4 and Materials and Methods). Surprisingly, we did not observe

any accumulation or decay of the quenchers in the µs range in PSII supercomplexes, indicating that S–T annihilation involving Car triplet states cannot be associated with the observed rather short fluorescence lifetimes in PSII with a closed RC and an unquenched antenna system. However, this experiment cannot exclude the generation of Car triplets leading to S–T annihilation in the presence of some additional quenching mechanism. The reason is that the excitation modulation technique relies on a change in the fluorescence lifetime, and therefore intensity, to monitor the accumulation and decay of a quencher. An example of the significant accumulation of Car triplets in an isolated antenna compared to the static result for a C_2S_2 supercomplex is shown in Fig. 6.14 in the SI.
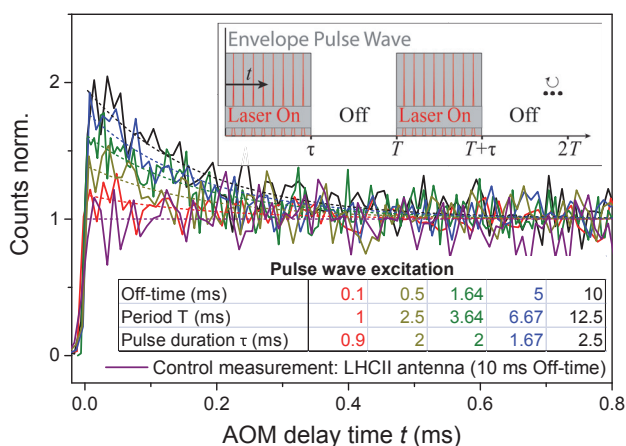

Figure 6.4: Fluorescence intensity kinetics of an exemplary single C_2S_2 complex for pulse wave excitation at the same excitation power but different Off-times in the ms range. These kinetics (AOM histograms) were extracted by histogramming the absolute fluorescence photon arrival times into one modulation cycle with a binning time of 10 µs. The dashed lines represent the fitted single exponential function of the form $F(t) = F_0 + F_1 e^{-k \cdot t}$ to extract the amplitude ratio F_1/F_0. The decay kinetics were normalized to $F_0 = 1$ (identical steady-state conditions). The inset illustrates the pulse wave excitation pattern used to investigate the fluorescence kinetics on the µs and ms timescale. The train of single laser pulses with a frequency of 76 MHz and a pulse width of about 200 fs is shown in red. The envelope modulation is shown in gray with a period T and a pulse duration τ.

The absence of any modulated kinetics being observed for single C_2S_2 supercomplexes in the microsecond range suggests that either the decay of the main quenching species is slower than microseconds or these quenchers accumulate much faster, *i.e.* that the signal disappears in a small fraction of the

first bin. The latter possibility was checked during a control experiment using lower excitation power and smaller binning times down to 20 ns, which resulted in the same flat behavior. However, at higher excitation intensities (above 150 W/cm^2) the kinetics do show the accumulation of Car triplets, coinciding with the already mentioned drop in the average lifetime, as shown in Fig. 6.13 in the SI.

Millisecond time scale.

By using the AOM modulation we can probe fluorescence kinetics not only in the microsecond range but also on the millisecond timescale. This allows us to check for longer lived quenching species in PSII supercomplexes. And we indeed found ms-kinetics in a significant fraction of complexes (>40%). However, different supercomplexes exhibited different relative amplitudes of the AOM kinetics; even for the same supercomplex the modulated fluorescence kinetics fluctuated significantly in time. Therefore, we chose to show just some exemplary kinetics in the following figures instead of the averaged data. The ms-range kinetics were observed in three biological replicates and more than 30 samples for each biological replicate. Some complexes did not show any ms kinetics, which indicates the presence of an even longer lived (*i.e.* >10 ms) or static quencher. This quencher could be located either in the antenna (with some LHC being in its permanently quenched conformation) or in the RC. An example of a ms-scaled AOM kinetics in a single C_2S_2 supercomplex, measured at 75 W/cm^2 pumping intensity, is shown in Fig. 6.4 and illustrates the dependence of the quenching kinetics on different Off-times of the laser modulation. Measuring the fluorescence amplitude recovery at different Off-times allows to estimate the time constant of the decay of the quenching species, as shown in Fig. 6.5 [202].

The exponential fit of the fluorescence recovery data results in a time constant of about 1–2 ms. This value would match the observed Chl triplet decay times in the RC of PSII with an oxidized quinone or doubly reduced Q_A[205], but not the PSII supercomplexes with closed RCs. Moreover, control experiments on LHCII trimers show a flat plateau on the ms timescale (see magenta curve in Fig. 6.4), which indicates that there is no light-dependent accumulation or decay of such Chl triplets in antenna complexes. The presence of any unquenched Chl triplets remaining in the antenna part of PSII cannot be fully neglected, however. Meanwhile, the fast kinetics of Car triplet accumulation (5 µs) in antenna complexes are averaged out on a ms timescale and therefore are hidden in the first time bin of the AOM histogram in Fig. 6.4.
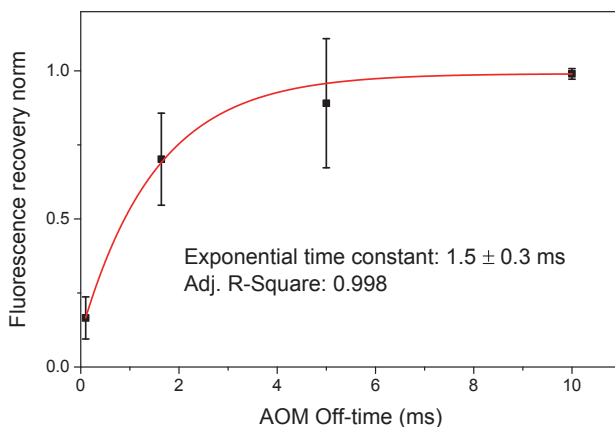
Figure 6.5: Illustration of the amplitude ratio F_1/F_0 (see Fig. 6.4 for definition), obtained from the AOM kinetics shown in Fig. 6.4 at different Off-times for five C_2S_2 supercomplexes. Only those supercomplexes that did not exhibit any accumulation of the static quenchers during the measurement time of more than a minute were analyzed, hence the low number of complexes. The amplitude ratio of each AOM decay curve is normalized to the maximum kinetics observed at an Off-time of 10 ms to allow the comparison of five complexes. Fitting these data points with an exponential saturation curve allows us to extract an approximate decay time constant of the quencher species.

Measuring ns time range kinetics during the ms modulation cycle.

If we now also utilize the time-tagged relative arrival time of fluorescence photons, we can create a two-dimensional histogram of both the AOM modulation delay time and the fluorescence decay time. The corresponding graph is shown in Fig. 6.6, where the color-coded small horizontal stripes represent the detected amount of fluorescence photons within a corresponding two-dimensional bin. The x-axis is exactly the same as in Fig. 6.4 and the y-axis depicts the fluorescence decay for each time bin of the AOM modulation. The vertical slices at two different AOM delay times (red and blue dashed lines) result in the fluorescence decay kinetics shown in the right panel of Fig. 6.6. The integral over the whole y-axis, as depicted in the top panel, yields the same AOM kinetics as shown with the black line in Fig. 6.4. In other words, Fig. 6.6 effectively illustrates the evolution of the fluorescence decay during an excitation modulation cycle. Surprisingly, this two-dimensional distribution reveals the presence of a long lifetime component in the nanoseconds range at early AOM delay times that disappears with the accumulation of the quencher. This
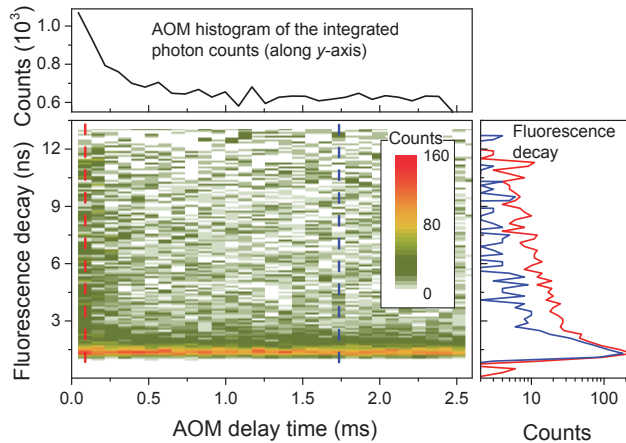
Figure 6.6: Two-dimensional representation of the arrival time of fluorescence photons relative to the pulse wave excitation on the *x*-axis (AOM delay time) and relative to the pulsed laser on the *y*-axis (Fluorescence decay). The On- and Off-time of the light modulation were 2.5 and 10 ms, respectively. The data is taken from the same exemplary complex as the black line in Fig. 6.4 but binned into intervals of 90 μs AOM delay time and 100 ps fluorescence decay time. These two-dimensional bins are color-coded to represent the absolute amount of detected photons. Most of the photon counts (white and light green bins) at AOM delay times above 0.5 ms and above a fluorescence decay time of 3 ns constitute dark counts and background signal. The top panel illustrates the integrated photon counts along the *y*-axis which results in an AOM histogram that is, apart from a different binning interval, identical to the black line shown in Fig. 6.4. The right panel illustrates the fluorescence decay slices (logarithmic *x*-axis) along the red and blue dashed lines in the main panel.

is an important result as it shows that during the dark period of the modulation cycle the PSII supercomplex is reversibly switching to an unquenched state with a closed RC. The fluorescence lifetime of this long decay component is on average $\tau_{long} = 3.5 \pm 0.5$ *ns* (standard deviation (SD), measured for 25 complexes), which is identical to the lifetime found in isolated LHCs. Its relative amplitude is only about 0.03 ± 0.02 (SD).

6.4 DISCUSSION

Possible quenchers in PSII

Our results indicate that the fluorescence decay of isolated PSII supercomplexes at the utilized excitation intensities is dominated by a time-dependent and par-

tially reversible quenching mechanism. Since the maximum turnover rate of photochemical quenching is about three orders of magnitude slower than the average absorption rate in confocal SMS experiments, the situation with open RCs seems very unlikely, so that all the RCs are closed within a few microseconds after starting the experiment. This result was further supported by the control measurements with added DCMU, which inhibits electron transfer to the secondary quinone Q_B, but had no influence on our measurements. In general, it is also possible that Q_A gets doubly reduced and protonated or even escapes entirely [206, 207]. As a result, the electrostatic effect of Q_A^- is not present then, and the rate of charge separation should remain similar to that of an open RC [208]. In such a case, charge recombination of the radical pair would also lead to a formation of Chl triplet states with the ms lifetimes [205], so that the observed fluorescence kinetics under our experimental conditions would then be dominated by S–T annihilation. Moreover, excitations are always efficiently quenched by the Chl triplet in the RC, which agrees with the lack of any reversible fluorescence kinetics and the absence of a long lifetime component for a significant fraction of PSII complexes. The accumulation of a doubly reduced and protonated quinone has indeed been demonstrated before for strong anaerobic illumination [209]. Such a scenario therefore seems to be a valid hypothesis to explain the lifetime of the fraction of complexes that do not show any ns-lifetime component. However, any other form of photoinhibition, pigment radicals, or permanently quenched complexes cannot be excluded either.

A very interesting outcome is the fact that under modulated excitation conditions PSII supercomplexes show a long lifetime component of about 3.5 ns at the onset of the AOM modulation cycle, which implies that the RC is closed in the beginning of each excitation cycle (see Fig. 6.6). In contrast, the fluorescence decay kinetics in PSII supercomplexes, measured continuously without the modulation, show no long lifetime component, as illustrated by the blue trace in the inset of Fig. 6.2B. Furthermore, only a PSII complex without any static quencher will exhibit a nanosecond lifetime component, thus there should not be any photoinhibition in the context of permanent quenching due to damaged pigments in the RC. This might seem surprising, but the turnover of the RC is slowed down by Q_A^- and further reduced by additional quenching mechanisms. Such a scenario is exactly the principle of photoprotection in native systems, which works even better in our anaerobic conditions, because not the triplet states alone but in combination with highly reactive singlet oxygen would be the main reason for photoinhibition in the RC [210, 211]. Under identical measuring conditions, isolated antennas remain unquenched up to

dozens of minutes [202]. However, in the regime of a closed RC with no additional quenching mechanism we theoretically expect a significant build-up of Car triplet states. This effect is consistent with the observation that even at time zero of the AOM histogram shown in Fig. 6.6, there is still a high fraction (>90%) of a fast decay component. This microsecond accumulation of Car triplets cannot be resolved with a millisecond modulation due to the lower number of cycle repetitions and detected photons. The subsequent decrease in fluorescence intensity during later times within the AOM histogram correlates with the disappearance of the nanosecond lifetime component. This implies the accumulation of a distinct quencher with a millisecond decay time. This quencher dominates the singlet excited state decay, thus reducing the number of Car triplets. The transient kinetics of Car triplet accumulation are hidden in the first bin of the ms AOM histograms, as already noted above.

What is the nature of the quenching mechanism that activates and decays on a millisecond timescale? The accumulation and subsequent decay of the Chl triplet states could possibly explain our data. However, it is known that the lifetime of these states is much shorter—about 7 μs—if Chl triplets are generated in closed RCs in the presence of a singly reduced quinone [205, 212]. On the other hand, Chl triplet states located somewhere in the antenna are efficiently quenched by a nearby carotenoid molecule. In fact, isolated light-harvesting complexes did not show any evidence for the presence of unquenched Chl triplets. The influence of Chl triplets on the modulated kinetics therefore seems to be unlikely.

Single LHCs, however, exhibit significant fluorescence blinking at the characteristic timescale of 10 ms, which is the limit of resolving individual intensity fluctuations, and most likely also at shorter times [46]. The cumulative effect of multiple blinking subunits of PSII (individual antenna complexes) will modulate the observed fluorescence intensity and the correlated average lifetime based on the specific diffusion distances needed for the excitations to reach some specific quenching site. Moreover, the timescale of fluorescence blinking follows a power-law behavior over multiple orders of magnitude of the delay times and has a tail reaching even seconds [46]. Our data indeed shows time-dependent fluctuations of the fluorescence lifetime and intensity on this slower and readily accessible timescale. The observed variations of the relative amplitude of the AOM kinetics, mentioned above, also support this hypothesis and suggest that this switching of individual LHCs is present even on shorter timescales. We note that in PSII the effect of fluorescence blinking is not as clearly visible as observed in an isolated antenna due to much longer diffusion times

spent by the excitation before it is trapped in some specific antenna complex being in its quenched conformational state.

Monte-Carlo simulations of excitation dynamics in PSII

In order to test the effect of a fluctuating antenna on the overall excitation dynamics in an isolated PSII complex, as discussed above, we proceeded with Monte-Carlo simulations of excitation energy transfer and quenching in PSII, based on a coarse-grained model of a C_2S_2 supercomplex [22, 213]. We accounted for the random generation of the Car triplet states within the antenna, responsible for S–T annihilation, as well as random switching of the antenna complexes between their light-harvesting and quenching conformations. During these simulations, we assumed a mean inter-complex excitation hopping time of 25 ps [94, 110, 200] and an excitation trapping time by the quenched antenna of 50 ps [62, 201]. The switching times of LHCs between their conformational quenched (*off*) and unquenched (*on*) were set to $k^{-1}_{off \to on} = 0.44$ ms and $k^{-1}_{on \to off} = 0.63$ ms, respectively. For other model parameters, chosen according to the results of SMS measurements on single LHCII complexes [83, 106], as well as details on the simulation procedure, see SI. Fig. 6.7A illustrates the resulting time evolution of the mean fluorescence lifetime, resembling fluorescence intensity fluctuations shown in Fig. 6.2B. The histogrammed distribution of these lifetimes, presented in Fig. 6.7B, also qualitatively fits with the experimental data. At each time point, the calculated excitation decay kinetics exhibited multi-exponential behavior, the corresponding distribution of their lifetimes and relative amplitudes are shown in Fig. 6.15A in the SI. From our simulations it also follows that under our experimental excitation conditions each C_2S_2 unit contained on average about 4.1 quenched light-harvesting antenna complexes and about 0.2 Car triplet states, see Fig. 6.15B. These results imply that the existence of quenched LHC domains is sufficient to explain the observed average lifetime with continuous laser excitation. They are furthermore consistent with SMS experiments on isolated antenna complexes and agree well with recently published works on a fluctuating antenna [94, 200, 201].

To properly describe the ms-ranged fluorescence kinetics measured during the excitation modulation, we assumed that the observed fluorescence intensity variations arise from the light intensity-dependent formation (and relaxation) of the quenched LHC domains. Fluorescence blinking in isolated LHCIIs is indeed dependent on the excitation intensity [46], which implies that the reversible switching of LHC domains into the quenched and unquenched level
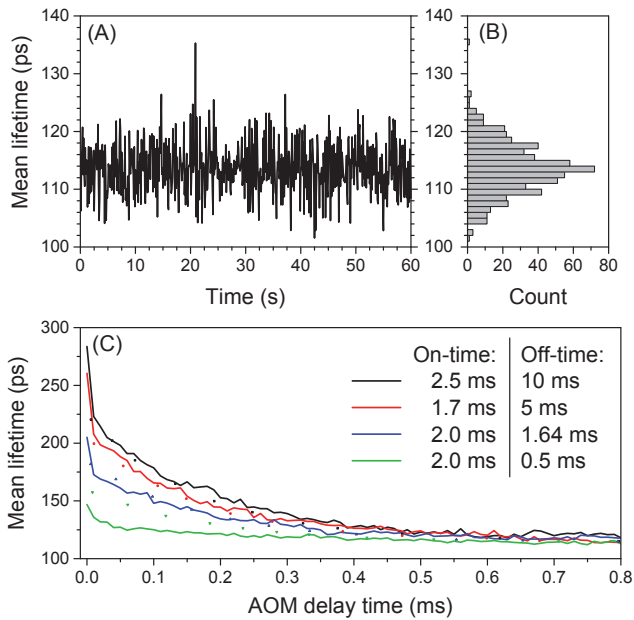
Figure 6.7: (A) Example of a simulated time trace of the mean excitation lifetimes in the coarse-grained model of a C_2S_2 supercomplex. (B) The histogram distribution of lifetimes shown in (A). (C) The simulated AOM kinetics (lines), exhibiting good agreement with the experimental result (dots, taken from Fig. 6.4).

is influenced by the light modulation. This can be modeled by adjusting the switching rate $k^{-1}_{on \to off}$ from 0.63 ms (for the continuous illumination discussed above) to 1.48 ms following a dark (laser off) period of 10 ms, which drops the mean number of quenched complexes from 4.1 to 2.3 just prior to the new AOM illumination cycle. The AOM fluorescence kinetics, obtained on a ms timescale under these assumptions and shown in Fig. 6.7C, reproduce the experimental results indeed reasonably well. An elaborate description of the simulation procedure and the postulated equation to account for the change in $k^{-1}_{on \to off}$ can be found in the the SI.

The profound effect of blinking subunits in a closed PSII supercomplex without any additional quenching mechanism, which is the most likely situation at much lower light intensities of natural sun light, can directly be seen from the significant change of the fluorescence decay kinetics during the AOM modulation cycle: the ns lifetime at early times of the AOM modulation decreases to a much shorter lifetime of about 100–150 ps in the presence of quenched LHCs. However, the probability for blinking events at physiological light conditions

(about 10^4 times smaller light intensity than under confocal SMS illumination) decreases significantly. On the other hand, this situation fits well with the thoroughly studied presence of multiple allosteric mechanisms to regulate qE. In other words, our results show the intrinsic capacity of the LHCs within a PSII supercomplex to switch reversibly between the conformational light-harvesting and quenched states as well as to sense light intensity variations by modulating the rates of this switching. Allosteric mechanisms associated with NPQ in native systems, *i.e.* the xanthophyll cycle, the role of PsbS and protein aggregation[26–28], can help to overcome the energy barrier to the quenched state at much lower and physiological light conditions. The fact that the fluorescence lifetime measured at an excitation intensity of 75 W/cm^2 is similar to that obtained under excitation power of 2.5 W/cm^2 (a factor of $\sim$ 37 above physiological high light conditions of about 2000 µmol photons $\cdot$ m$^{-2} \cdot$ s^{-1}) and is furthermore comparable to usual ensemble measurements at physiological excitation conditions illustrates that our results are also relevant to the processes happening *in vivo*. The presence of oxygen in native photosynthesis aggravates the harmful potential of triplet states but should otherwise not influence energy transfer kinetics.

6.5   CONCLUSIONS

In conclusion, we directly measured and then successfully modeled the effects of a fluctuating antenna system on the mean excitation lifetime in single PSII supercomplexes. Our results are also consistent with the migration-limited model, where the average fluorescence lifetime of PSII is dominated by the diffusion of excitations through the antenna system to the RC or any other trap [16, 71, 214]. The AOM kinetics (compare Figs. 6.4 and 6.6) represent the reversible and excitation-intensity dependent switching of LHC domains between a quenched and unquenched state. Such conformational dynamics has recently been linked to NPQ within the concept of a fluctuating antenna system [201]. The observed changes in fluorescence intensity and lifetime can therefore effectively be interpreted as a brute-force measurement of qE. Our use of modulated light illumination is analogous to the established pulse-amplitude modulation (PAM) technique to measure the photoprotective response of photosynthetic organisms. The conformational changes associated with NPQ in native systems are induced by allosteric and partially redundant mechanisms. We propose, that alternative strong illumination provides enough excess energy to randomly access and explore such intrinsic conformations on a fast timescale. Our work

thus directly illustrates, how environmental control over a fluctuating antenna can regulate light-harvesting in plant photosynthesis.

6.6 SUPPORTING INFORMATION

Monte-Carlo simulations of fluorescence blinking in a single C$_2$S$_2$ supercomplex

Continuous illumination regime

For simplicity, the excitation dynamics in a C$_2$S$_2$ supercomplex was analyzed in terms of a coarse-grained model (see Fig. 6.8A) by implicitly taking into account only inter-complex excitation transfer while totally neglecting fast excitation equilibration within the same pigment–protein complex [22, 213]. Conventionally, the excitation dynamics in such photosynthetic systems is described by solving the Pauli Master equations:

$$\frac{\mathrm{d}P_i}{\mathrm{d}t} = \sum_{j \neq i} k_{i \leftarrow j} P_j - \sum_{j \neq i} k_{j \leftarrow i} P_i - k_{\mathrm{rel}}^{(i)} P_i,$$

where $P_i(t)$ is the time-dependent population of the ith complex, $k_{i \leftarrow j}$ is the excitation "hopping" rate from the jth to the ith complex, and $k_{\mathrm{rel}}^{(i)}$ is the excitation relaxation rate in the ith complex due to fluorescence, non-radiative dissipation, photochemical trapping (in RCs) or any other quenching mechanism. On the other hand, such a simple kinetic approach is not suitable to describe non-linear singlet–singlet or singlet–triplet annihilation processes occurring in small molecular systems like LHCII trimers—more sophisticated statistical model should be used instead [75, 76, 91, 106]. This model was proven to correctly describe the experimentally observed non-exponential kinetics, but it scales rapidly with the number of the states available per system [91, 106] and is therefore computationally inadequate for larger systems. A single PSII supercomplex, however, is an example of the intermediately sized molecular aggregate, for which a conventional kinetic approach cannot be used in the non-linear regime and which, at the same time, is too large for the statistical model to be applied. Therefore, in order to deal with these effects, we used a Monte-Carlo (MC) approach to simulate fluorescence blinking in single PSII supercomplex arising due to a random generation of the triplet states (resulting in the non-linear singlet–triplet annihilation on a microsecond timescale) and, as will be shown below, random generation of the static traps resembling NPQ quenchers observed *in vivo*.

Table 6.1: Model parameters used for MC simulations of fluorescence blinking in a C_2S_2 supercomplex.

Model parameter	Value
Inter-complex excitation hopping time [94, 110, 200]	$k_h^{-1} = 25\,\text{ps}$
Singlet excitation dissipation time [106]	$k_{dis}^{-1} = 3.5\,\text{ns}$
Triplet excitation generation time [106]	$k_{ISC}^{-1} = 8.5\,\text{ns}$
S–T annihilation time within a complex	$\gamma_{ST}^{-1} = 5\,\text{ps}$
Triplet state decay time [106]	$K_T^{-1} = 9\,\mu\text{s}$
Time delay between two subsequent pump pulses	$\tau = 13.16\,\text{ns}$
Absorption cross-section of C_2S_2 supercomplex	$\sigma = 7 \cdot 10^{-15}\,\text{cm}^2$
Probability for antenna complex to be in a quenched state	$w = 41\%$
Excitation trapping time by the antenna complex in a quenched state [62, 201]	$k_{NPQ} = 50\,\text{ps}$

All major parameters used for our MC simulations of excitation dynamics in a C_2S_2 supercomplex are listed in Table 6.1. Based on the experimental conditions—the mean absorption cross-section of the C_2S_2 supercomplex ($\sigma = 7 \cdot 10^{-15}\,\text{cm}^2$), the laser repetition rate ($f = 76\,\text{MHz}$), and the excitation wavelength (633 nm)—the mean number of the absorbed photons per pulse under the $75\,\text{W/cm}^2$ pumping intensity was assumed to be $n_0 = 0.022$. Thus, during the simulations, we generate an excitation in a randomly chosen ith complex. Then, for each time step $\Delta t = 5\,\text{ps}$ we calculate the probabilities for excitation energy transfer to any randomly chosen neighboring jth complex, $k_{j \leftarrow i}\Delta t$, and that for the excitation relaxation, $k_{rel}\Delta t$. The rate $k_{j \leftarrow i}$ was related to the mean excitation "hopping" rate k_h (shown in Table 6.1) by re-scaling it for the varying number n_i of Chl a pigments in different antenna complexes [22, 213]:

$$k_{j \leftarrow i} = k_h \cdot \begin{cases} 1, & n_i < n_j, \\ \frac{n_j}{n_i}, & n_i \geq n_j. \end{cases}$$

Meanwhile, the relaxation rate k_{rel} was chosen to be $k_{dis} = (3.5\,\text{ns})^{-1}$ unless there was a triplet state previously generated in that particular ith complex; in the latter case, the relaxation rate was set to the S–T annihilation rate, γ_{ST}. In our previous work on S–T annihilation in single LHCII trimers [106], the obtained

annihilation time of ~35 ps also contained the time needed for the excitation to equilibrate over the whole trimer (basically the hopping time). Therefore, in the current simulations we set the intrinsic annihilation time for each complex containing the triplet state to $\gamma_{ST}^{-1} = 5$ ps. If an excitation exhibited a linear relaxation (k_{dis}), a triplet state in the corresponding complex was generated with a probability $k_{ISC}/k_{dis} \approx 41\%$. In accordance to our previous work, we also assumed that the resulting chlorophyll triplet state was then quickly transferred to the nearby carotenoid, where it survived on average for a time period of $K_T^{-1} = 9$ µs.

As a result, excitation dynamics was simulated until the excitation was dissipated in one of the complexes at some particular time t_i. Then the population kinetics for the corresponding realization was defined as

$$p_i(t) = \begin{cases} 1, & t \leq t_i, \\ 0, & t > t_i. \end{cases}$$

The final obtained population kinetics after N random realizations was calculated as $P(t) = \frac{1}{N} \sum_i p_i(t)$.

Since photochemical quenching in closed RCs can be neglected [132], one would expect a considerable accumulation of triplet states, which could explain a pronounced decrease of the excitation mean lifetime from ~3.5 ns (separate LHCIIs) down to the observed ~115 ps in single C_2S_2 supercomplexes. Our MC simulations, based on the above-mentioned rates, indeed revealed that in a steady-state regime there are on average 1.16 triplet states generated per PSII. This number, however, is still too small since it reduces the mean excitation lifetime just to ~650 ps. Thus, in order to achieve the experimentally observed ~115 ps, one needs to postulate the presence of some additional long-lived excitation traps resembling NPQ quenchers.

Single-molecule spectroscopy of LHCII trimers revealed the ability of the latter to switch between several conformational states, which were shown to be related to NPQ [46, 47, 78]. Therefore we assumed that during the fluorescence measurements in C_2S_2 supercomplexes, each LHCII monomer (or minor antenna complex as well) on a µs timescale could randomly switch between the dominating light-harvesting and rarer quenching state (*off*-states). During the simulations, such a switching possibility was considered every 10 µs. Based on the recent temperature-dependent time-resolved fluorescence measurements in LHCII trimers and aggregates that revealed the "energetic deepness" of this quenched states [201], we chose the excitation trapping time by the quenched

complexes and the excitation escape time from these complexes back to the antenna to be equal to 50 ps and 1 ns, respectively.

Introduction of these additional trapping centers, concurring with S–T annihilation, has notably reduced the mean steady-state concentration of triplet states within the C_2S_2 supercomplex. Thus, in order to reduce the mean excitation lifetime down to ~115 ps, we had to assume that there is a $w = 41\%$ probability for each of 10 antenna complexes (6 monomeric LHCII subunits and 4 minor antenna complexes, see Fig. 6.8) to be found in the quenching state and, accordingly, 59% probability for the light-harvesting state. This can help us to evaluate the ratio of the *on↔off* (light-harvesting ↔ quenched state, respectively) switching rates for a single complex:

$$\frac{k_{\text{on}\to\text{off}}}{k_{\text{off}\to\text{on}}} = \frac{w}{1-w} \approx 0.7,$$

The absolute values of these rates, which still remain undefined, determine the mean square deviations of the resulting mean lifetime, averaged over some binning time ΔT: slower switching rates increase the duration of the random realizations of the traps distributed over the C_2S_2 antenna, corresponding to either smaller or larger concentration of the quenching sites. The results of the MC simulations, obtained by assuming $k_{\text{on}\to\text{off}}^{-1} = 0.63\,\text{ms}$ and $k_{\text{off}\to\text{on}}^{-1} = 0.44\,\text{ms}$, are presented in Figs. 6.7A,B and 6.15.

The time evolution of the calculated mean excitation lifetimes, which were averaged over a $\Delta T = 100\,\text{ms}$ interval and are proportional to the actually observed fluorescence intensity, are shown in Fig. 6.7A, and the statistical distribution of these lifetimes is demonstrated in Fig. 6.7B. The corresponding time trace of the mean number of the NPQ and triplet states is shown in Fig. 6.15B. As already mentioned, on average 4.1 NPQ quenchers per C_2S_2 supercomplex were needed to achieve the substantial drop in the mean excitation lifetimes, whereas the mean number of triplet states due to concurrence with the NPQ traps was reduced to ~0.2. Random fluctuations of the number of NPQ and triplet states results in the fluctuations of the mean excitation lifetimes and, therefore, of the excitation decay kinetics. The multi-exponential decay behavior, requiring up to 3 different lifetimes, can be clearly observed; the distribution of these lifetimes, together with their relative amplitudes, is shown in Fig. 6.15A. The ns component obviously corresponds to some rare realizations, when almost no NPQ traps or triplet states were formed.

AOM regime

The MC simulations of the fluctuating mean excitation lifetimes demonstrated the presence of some additional static traps resembling NPQ quenchers and allowed us to evaluate their mean concentration, *i.e.* the ratio of the switching rates between two different conformational states of the pigment–proteins: $k_{\text{on}\rightarrow\text{off}}/k_{\text{off}\rightarrow\text{on}} \approx 0.7$. The absolute values of these switching rates, currently remaining undefined, can be evaluated by modeling the AOM kinetics in the C_2S_2 supercomplex on the ms timescale. Since the formation of any triplet states and the equilibration of their mean concentration per C_2S_2 supercomplex is assumed to occur within the initial part of the AOM kinetics, the experimentally observed change in the fluorescence intensity on a timescale of hundreds of µs can be attributed only to the formation and relaxation of the NPQ quenchers. We can assume that during laser excitation the quenched state of the pigment–protein complexes becomes more favorable, and the mean number of the NPQ traps increases, leading to the drop in the fluorescence kinetics, observed in the AOM kinetics on a ms timescale. On the other hand, during the dark modulation period the probability for the antenna complex to switch into the quenched state decreases. As a result, at the onset of each AOM illumination cycle we observe a notable increase in the fluorescence intensity. In other words, the external light field acts as a modulator between the different conformational states of the LHCs. Schematically these processes are demonstrated in Fig. 6.16A.

The AOM kinetics, corresponding to the longest AOM illumination-Off time (10 ms), can be obtained in a most straightforward way—in this case, from the experimental kinetics we see that the initial fluorescence intensity (at the onset of the illumination period) is almost twice as large as the steady-state one. This means that during the preceding illumination-Off period the concentration of NPQ traps should exhibit approximately a two-fold decrease, so that the ratio $k_{\text{on}\rightarrow\text{off}}/k_{\text{off}\rightarrow\text{on}}$ should decrease down to ~0.35. Then, during the AOM illumination-On period this ratio should gradually increase back to 0.7, leading to the formation of additional NPQ traps and resulting in the drop of the AOM kinetics. As a result, under continuous illumination there are about 4 NPQ traps, and when the illumination is turned off, the mean number of NPQ reduces to ~2–2.5.

For simplicity, in our simulations we assumed that the $k_{\text{off}\rightarrow\text{on}}$ rate (red arrow in Fig. 6.16A) always remained unchanged, and all the observed intensity variations were related to the changes in $k_{\text{on}\rightarrow\text{off}}$ (*cf.* blue and green arrows in Fig. 6.16A). Moreover, we assumed that at the onset of the AOM illumination the switching rate instantaneously increased from $k'_{\text{on}\rightarrow\text{off}}$ (dark-adapted sys-

tem) to $k_{\text{on}\rightarrow\text{off}}$ (light-adapted system). Such an instantaneous increase, however, does not lead to the instantaneous increase of the concentration of the NPQ traps since the *on↔off* switching rates are finite, and it takes some time for the system to reach the new equilibrium. This allows us to evaluate the absolute values of these switching rates: if they were very fast, the AOM kinetics would drop from its maximal value to the steady-state plateau very rapidly. On the other hand, too slow switching rates would result in too slow kinetics. Thus, in order to follow the experimental kinetics, we had to define the rates as follows: $k^{-1}_{\text{off}\rightarrow\text{on}} = 0.44\,\text{ms}$, $k^{-1}_{\text{on}\rightarrow\text{off}} = 0.63\,\text{ms}$, and $k'^{-1}_{\text{on}\rightarrow\text{off}} = 1.48\,\text{ms}$. If the increase from $k'_{\text{on}\rightarrow\text{off}}$ to $k_{\text{on}\rightarrow\text{off}}$ were not instantaneous, these rates should be somewhat faster. Therefore the timescales listed above define the lower limit for these switching times. The resulting AOM kinetics, calculated using these assumption, is shown with a black line in Fig. 6.7C in the main text and demonstrates a rather good quantitative correspondence to the experimentally measured kinetics (*cf.* black squares in Fig. 6.7C). As before, we present the time evolution of the mean fluorescence lifetime, which is proportional to the fluorescence intensity directly observed in our measurements. There is a sharp peak in Fig. 6.7C (just the two initial points) in the simulated AOM kinetics at the onset of AOM illumination period. As it follows from Fig. 6.14A, presenting the time evolution of the mean number of triplet states, this peak appears since initially the concentration of triplet states is 0 (leading to higher fluorescence intensity), and then it rapidly increases during the first 10–20 μs, opening another channel for excitation relaxation due to S–T annihilation. Finally, the black line in Fig. 6.14B demonstrates the gradual increase of the mean number of the NPQ traps from ~2.3 to ~4.1 during the illumination period.

As discussed above, we assumed an instantaneous increase of the *on→off* conformational switching rate at the onset of the illumination period. A similar assumption about the instantaneous decrease of this rate when the illumination was turned off, however, resulted in absolutely the same AOM kinetics, calculated for other experimentally assessed AOM cycle periods. On the other hand, a much better quantitative description was obtained by postulating that this opposite process takes some time and the $k_{\text{on}\rightarrow\text{off}}$ rate in dark conditions increases according to the following equation:

$$k_{\text{on}\rightarrow\text{off}}(t) = k_{\text{min}} + \frac{k_{\text{max}} - k_{\text{min}}}{1 + t/\tau},$$

here t is the time period spent in the dark, $k^{-1}_{\text{min}} = 1.7\,\text{ms} \gtrsim k'^{-1}_{\text{on}\rightarrow\text{off}}$, $k_{\text{max}} = 0.63 = k^{-1}_{\text{on}\rightarrow\text{off}}$, and $\tau = 0.7\,\text{ms}$. This dependence, being faster than the similar

exponential distribution for small t values and slower than an exponential function for larger t, is shown as a blue line in Fig. 6.16B. With such a function, the AOM kinetics for other AOM illumination cycles were calculated (colored lines in Figs. 6.7C and 6.14).
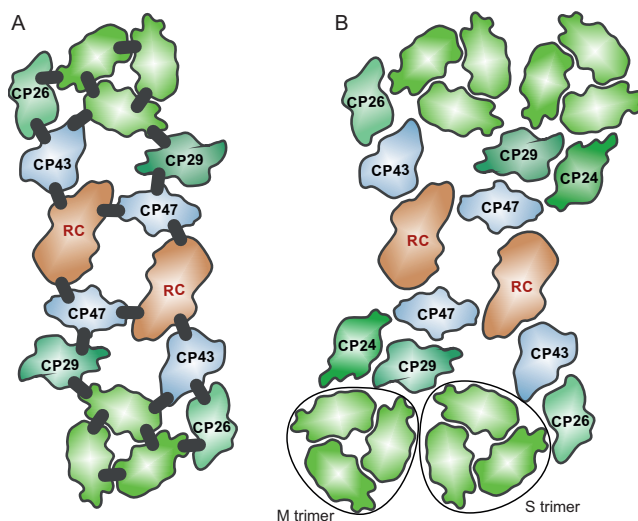

Figure 6.8: Schematic structure of a C_2S_2 (A) and $C_2S_2M_2$ (B) supercomplexes. The unlabeled light green complexes correspond to the monomeric subunits of the LHCII trimers. Thick gray bars in (A) represent inter-complex excitation transfer pathways used in the coarse-grained modeling.
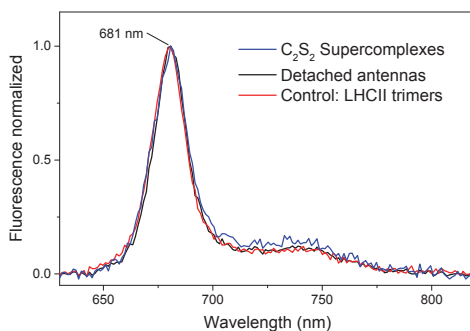
Figure 6.9: Averaged fluorescence emission spectra of C_2S_2 supercomplexes (blue line), from supercomplexes detached antennas (black line) and isolated LHCII trimers (red line). Each normalized spectrum is an average of about 30 individually measured complexes.
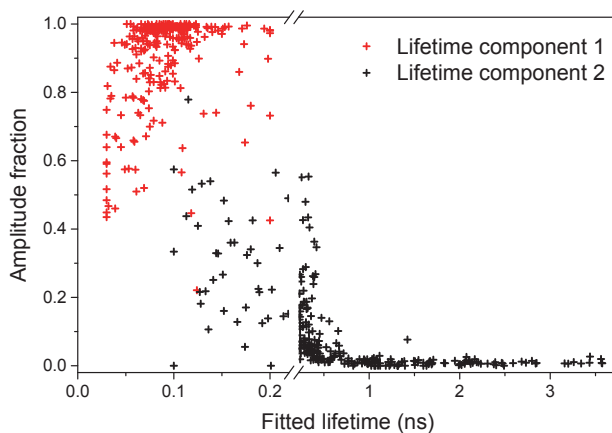
Figure 6.10: The distribution of the two fitted fluorescence decay exponential components of 33 C_2S_2 supercomplexes (about 250 intensity states)—a dominating one in the range of 100 ps and a slower one accounting for the lifetimes up to 3.7 ns.
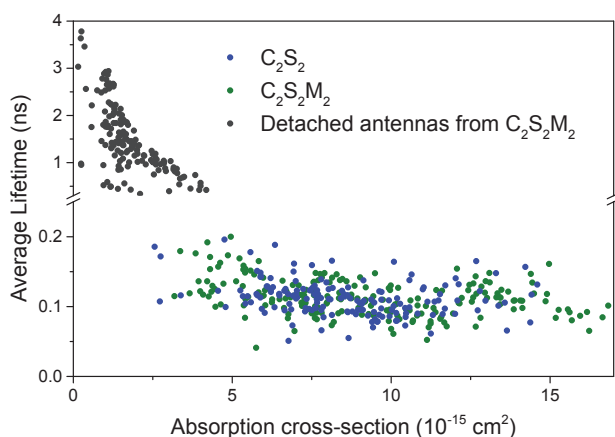
Figure 6.11: The relationship between the average fluorescence lifetime and the estimated absorption cross-section of individual complexes, resulting in different clusters representing PSII supercomplexes (blue and green circles) and detached antenna complexes (black circles). The presented data is the same as the one used in Fig. 6.3. The distribution of antenna complexes might even further be clustered into monomeric CP24, trimeric LHCII and possibly pentameric LHC complexes (LHCII trimer + CP24 + CP29). The width of the distributions shown in Fig. 6.12 in the SI illustrates the fitting error that does not allow the exact size determination of single complexes.
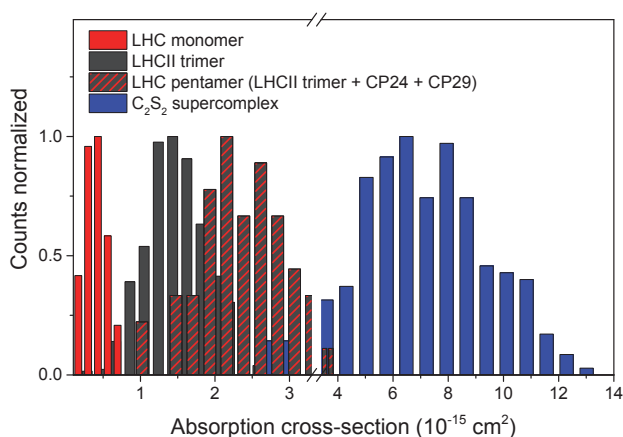
Figure 6.12: Histogram distributions of the calculated relative absorption cross-section of C_2S_2 supercomplexes (blue bars) and three reference samples. The red bars depict LHC monomers (CP24), the black bars relate to LHCII trimers, and the black bars with red stripes stand for LHC pentamers (LHCII trimer + CP24 + CP29). Note the break and change in scaling on the x-axis. The number of analyzed complexes per sample: 30 C_2S_2 supercomplexes, 20 LHC pentamers, 50 LHCII trimers and 45 LHC monomers.
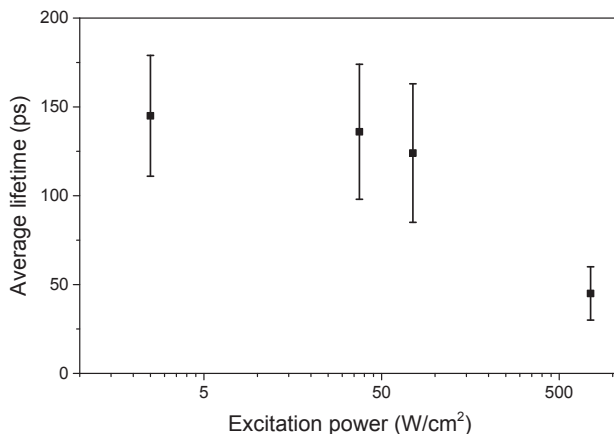
Figure 6.13: Excitation power dependence of the average lifetime of 25 C_2S_2 super-complexes on a semi-logarithmic scale. The error bars indicate the standard deviation obtained by analyzing more than 30 complexes at each excitation power.
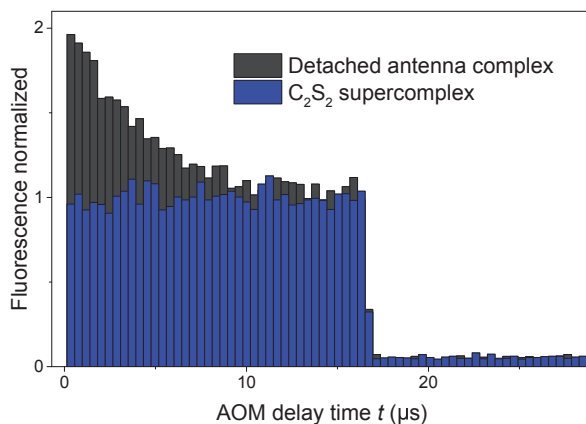

Figure 6.14: Exemplary AOM histograms of a detached light-harvesting antenna complex (black bars) and a C_2S_2 supercomplex (blue bars). The black bars illustrate the accumulation of Car triplets during the periodic illumination from 0 to about 17 μs. Those triplets can decay during the dark period in between the illumination cycles. The PSII supercomplexes do not show any fluorescence kinetics on that timescale.
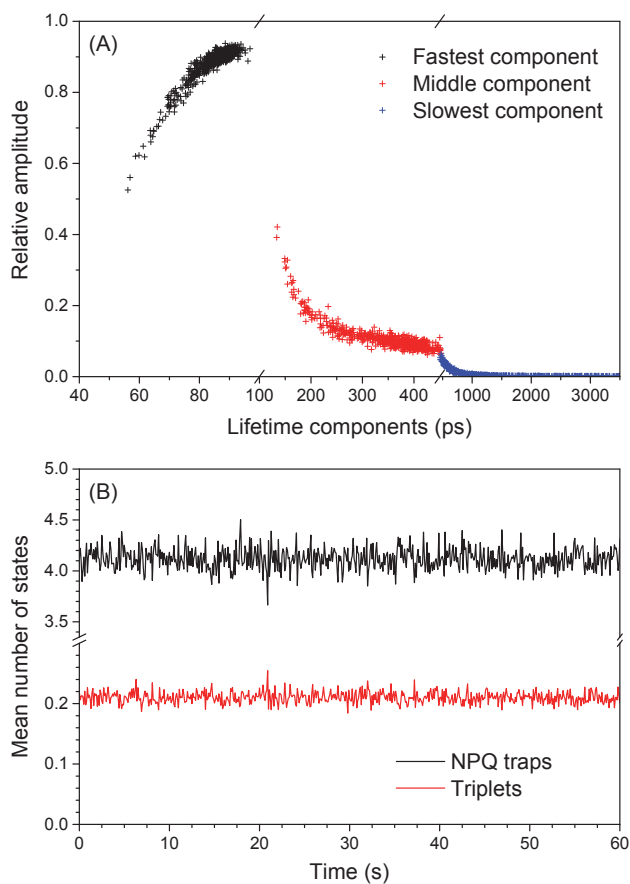
Figure 6.15: (A) Distribution of the lifetime components and their relative amplitudes, obtained from a 3-exponential fit of the excitation decay kinetics calculated at different points of the time trace in Fig. 6.7A. (B) Time evolution of the mean mean number of the triplet and NPQ states per C_2S_2 supercomplex, corresponding to the time trace shown in Fig. 6.7A.
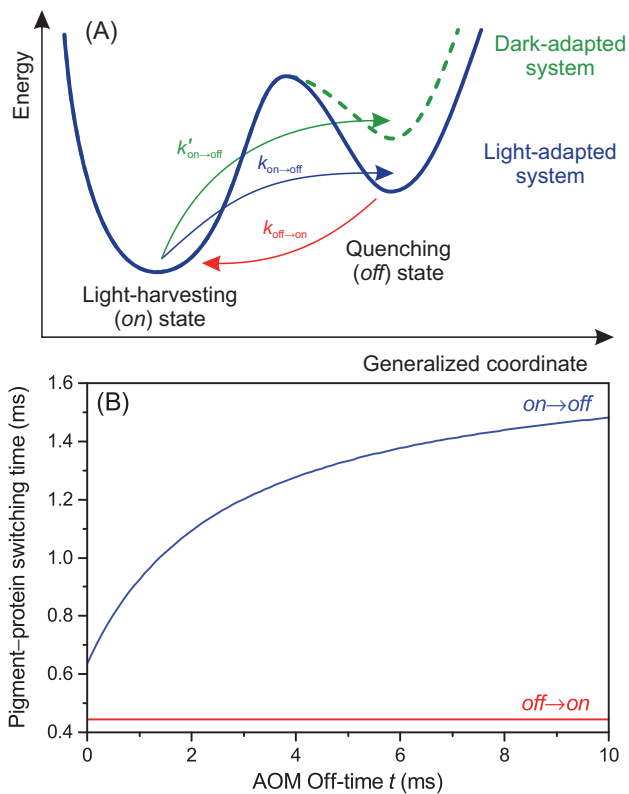
Figure 6.16: (A) Schematic presentation of the conformational light-harvesting and quenching states and the switching rates between them. The solid line corresponds to the illuminated system, and the dashed lines to the dark-adapted one, in which the probability of the quenching state is notably reduced. Color arrows denote the corresponding *on↔off* switching rates. (B) Switching times of the pigment–protein as a function of the time spent in dark conditions, used to calculate AOM kinetics shown in Fig. 6.7C.